Molecular Physics, 2014
Vol. 112, No. 14, 1929–1937, http://dx.doi.org/10.1080/00268976.2013.874601

Taylor & Francis
Taylor & Francis Group

RESEARCH ARTICLE

Optimal laser pulse design for transferring the coherent nuclear wave packet of H_2^+

Jun Zhang[a], Guang-Qiang He[b] and Feng He[c,*]

[a]*Joint Institute of UMich-SJTU and Key Laboratory of System Control and Information Processing (Ministry of Education)Shanghai Jiao Tong University, Shanghai, China;* [b]*State Key Lab of Advanced Optical Communication Systems and Networks, and Department of Electronic Engineering, Shanghai Jiao Tong University, Shanghai, China;* [c]*Key Laboratory for Laser Plasmas (Ministry of Education) and Department of Physics and Astronomy, Shanghai Jiao Tong University, Shanghai, China*

(*Received 22 September 2013; accepted 29 November 2013*)

Within the Franck–Condon approximation, the single ionisation of H_2 leaves H_2^+ in a coherent superposition of 19 nuclear vibrational states. We numerically design an optimal laser pulse train to transfer such a coherent nuclear wave packet to the ground vibrational state of H_2^+. Frequency analysis of the designed optimal pulse reveals that the transfer principle is mainly an anti-Stokes transition, *i.e.* the H_2^+ in $1s\sigma_g$ with excited nuclear vibrational states is first pumped to $2p\sigma_g$ state by the pulse at an appropriate time, and then dumped back to $1s\sigma_g$ with lower excited or ground vibrational states. The simulation results show that the population of the ground state after the transfer is more than 91%. To the best of our knowledge, this is the highest transition probability when the driving laser field is dozens of femtoseconds.

Keywords: coherent control; hydrogen molecular ion; ultrafast

PACS: 33.80.Rv; 42.50.Hz; 02.30.Yy

1. Introduction

Controlling coherent quantum states has been a longstanding goal since the invention of laser pulses. With the rapid advance of technology in recent years [1], researchers can now fine-tune the laser parameters to control the ultrafast processes inside atoms and molecules [2–4]. For example, by varying the relative phase of a two-colour (ω-3ω) laser field with ω the fundamental angular frequency, the target molecule may be constructively or destructively excited by simultaneously absorbing the ω and 3ω photons [5]. Another example is to change the time delay between two laser pulses so that the molecule can be first pumped to an intermediate state, then evolves and accumulates the time-dependent phases, and later be dumped to a different final state, thereby changing the production of a chemical reaction [6]. Furthermore, specific tailoring of the laser field may dictate a complex chemical reaction to follow one particular channel and stay away from all the others, achieving a selective terminal state [7]. Most recently, thanks to the phase-stabilised few-cycle laser pulse [8], the directional emission of an ionised electron [9], or the charge-direct transfer between nuclei [10,11] also become possible. The attosecond pulse may be used to selectively excite or ionise the target at unprecedentedly precise timing during the chemical reactions [12–14], and thus helps understanding the time-resolved fundamental physics.

As the simplest neutral molecule, H_2 (or D_2) is often chosen as a prototype system to be controlled and analysed. In the past few decades, the basic processes for H_2 exposed in strong laser fields have been extensively studied. As shown in Figure 1, the single-photon ionisation of H_2 may leave with a molecular ion H_2^+ in $1s\sigma_g$ state [15], whose nuclear wave function distribution may be described by the Franck–Condon approximation [16]. In this case, the initial nuclear wave packet (NWP) of H_2^+ is the same as the ground state of H_2, and it evolves along the $1s\sigma_g$ potential curve, as shown in Figure 2(c) [17]. Note that the H_2^+ nuclear wave packets shift to lower vibrational states as compared to the Franck–Condon distribution if the neutral molecule is tunnelling ionised [18,19]. In this paper, we want to demonstrate the feasibility of the optimisation algorithm, which does not depend on the concrete initial wave packet distribution sensitively. Therefore, we only consider the initial states with the Franck–Condon distribution. If a time-delayed probe pulse is subsequently introduced, H_2^+ may dissociate through the laser-induced coupling between $1s\sigma_g$ and $2p\sigma_u$ states [11,20–23], whose electronic wave functions have gerade and ungerade symmetry, respectively. The superposition of $1s\sigma_g$ and $2p\sigma_u$ states will induce an asymmetric electron localisation [12,24–33]. Alternatively, H_2^+ may also be ionised by the probe pulse, which leads to the Coulomb explosion [15,34]. The internuclear

* Corresponding author. Email: fhe@sjtu.edu.cn

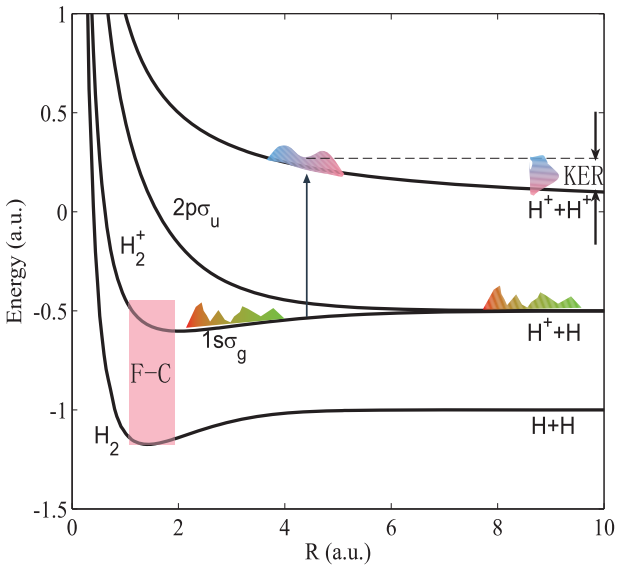

Figure 1. (Colour online) The schematic picture for the interaction between laser pulses and H_2. Four curves from bottom up are the potential curves for H_2, H_2^+ in $1s\sigma_g$, H_2^+ in $2p\sigma_u$, and coulomb explosion. F-C remarks the Franck–Condon transition area. The single ionisation of H_2 produces the H_2^+ in $1s\sigma_g$, followed by the dissociative ionisation by the probe pulse. The kinetic energy release (KER) reflects the information when the coulomb explosion happens.

distance at the instant when the ionisation of H_2^+ takes place can be reflected by the kinetic energy release (KER) of the Coulomb-explosion fragments [35–38]. In addition to these non-electron correlation processes, the first ionised electron may come back and rescatter with H_2^+, accompanying with the excitation of H_2^+ [39,40] and high harmonic generation [41], or auto-ionisation [42]. If the laser environments are appropriate, the single ionisation of H_2 may leave the H_2^+ in higher excited electronic states, e.g. $2p\sigma_u$ [14] or $2p\pi_u$ [43].

In these processes, the complexity of the H_2^+ NWP makes the whole process even more complicated. After the single ionisation, the NWP of H_2^+ is a superposition of 19 vibrational states with negligible auto-dissociative states. Each vibrational state has a different spatial distribution. Once the molecule is dissociated or ionised, each vibrational state also contributes a different KER to the molecular fragments [44]. The coherent superposition of the vibrational states may partly smear the asymmetric electron localisation [33], or lead to the time-dependent dissociation [45]. Since the stationary nuclear state can significantly simplify the physical picture, it is often desired to transfer the coherent NWP to one stationary state, especially to the ground vibrational state of H_2^+.

For the hetero-nuclear molecular ion HD^+, the permanent dipole induced by the asymmetric nuclear mass may

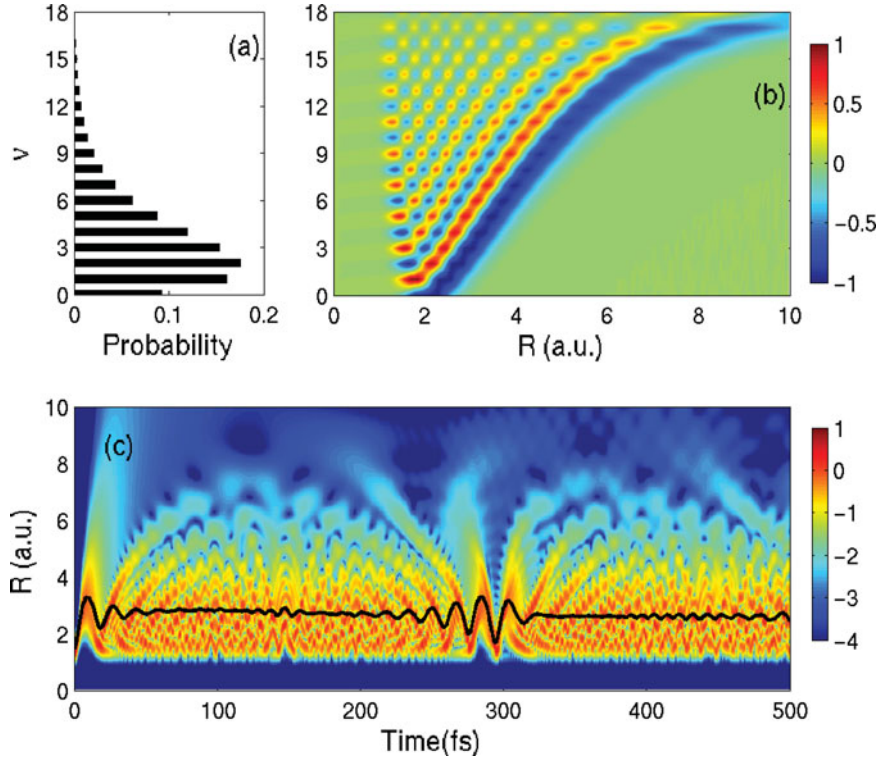

Figure 2. (Colour online) (a) Franck–Condon coefficients of the NWP of H_2^+. (b) Wave functions for the 19 vibrational states (in linear scale). (c) The free propagation of the Franck–Condon NWP of H_2^+ in the $1s\sigma_g$ potential curve (in logarithmic scale).

transfer the Franck–Condon NWP to the ground vibrational state [46]. However, for H_2^+, the external laser field has to be applied. Niederhausen and Thumm suggested to use the multi-pulse protocol to control the Franck–Condon coherent NWP and found that in the final coherent population, the largest proportion for a certain vibrational state can exceed 60% [47]. Niikura *et al.* studied to exert a laser-induced dipole force at an appropriate time to achieve up to 50% population for the ground vibrational state [48]. Picon *et al.* proposed to use a chirped few-hundred-femtosecond pulse or pulse train to transfer the first and second excited vibrational states to the ground vibrational state with the proportion up to 90% [49]. Bryan *et al.* used the pump-modify-probe strategy to manipulate the vibrational states, where the time-delayed second pulse may modify the relative populations of different states [50].

In this paper, we use optimal control theory to numerically design a laser pulse train to tailor the coherent vibrational states. We formulate it as a minimax problem with bounded constraints, and then apply sequential linear programming algorithm [51] to solve it. The gradient of the performance metric with respect to the laser pulses can be derived in an analytic manner, which facilitates the numerical computation. The major advantage of this approach is that it can explicitly handle the bound constraints on the control pulses. For the initial Franck–Condon NWP, the transfer to the ground vibrational state is achieved with the population more than 91%.

2. Numerical model

2.1. Two-channel equation

Consider the case that the single ionisation of H_2 produces a free electron and a molecular ion H_2^+ in $1s\sigma_g$, where the NWP of H_2^+ is described by the Franck–Condon approximation. If the time-delayed probe pulse is introduced to cause the dissociation, the dynamics is mainly governed by a two-channel equation (atomic units are used unless otherwise stated)

$$i\frac{\partial}{\partial t}\begin{pmatrix}\psi_g(R,t)\\ \psi_u(R,t)\end{pmatrix} = \begin{pmatrix} T_R + V_g(R) & d_{gu}(R,t)E(t)\\ d_{gu}(R,t)E(t) & T_R + V_u(R)\end{pmatrix} \times \begin{pmatrix}\psi_g(R,t)\\ \psi_u(R,t)\end{pmatrix}, \quad (1)$$

where $\psi_g(R, t)$, $\psi_u(R, t)$ are the NWP corresponding to the electron in $1s\sigma_g$ and $2p\sigma_u$ states, and $V_g(R)$, $V_u(R)$ are the potential curves for $1s\sigma_g$ and $2p\sigma_u$ states, respectively. The dipole coupling matrix between these two states is represented by d_{gu}, and $T_R = -\frac{1}{2M}\frac{\partial^2}{\partial R^2}$ is the second-order differential operator, where $M = 918$ is the reduced mass of two nuclei. The molecular rotation is neglected since we limit the pulse duration within a few tens of femtoseconds. The initial NWP is given by

$$\psi_g(R,0) = \psi_{Gr}^0(R), \quad \psi_u(R,0) = 0, \quad (2)$$

where $\psi_{Gr}^0(R)$ is the ground state of H_2. We use the Split-Operator method [52] to solve Equation (1). The R spans from 0 to 40, and the spatial step $\Delta R = 0.04$. The time step is set as $\Delta t = 1$. Mask functions are used to suppress the unphysical reflection by the boundary of the simulation box.

Our objective is to design a laser pulse E such that at the terminal time T_f, ψ_g can be transferred to the ground state of H_2^+, i.e.

$$\psi_g(R,T_f) = \psi_g^{\nu=0}(R), \quad (3)$$

where ν is the index of the vibrational state. The initial NWP $\psi_g(R, 0)$ is mainly a superposition of 19 vibrational states. By projecting it to the vibrational eigenstates of H_2^+, we obtain the Franck–Condon coefficients, as shown in Figure 2(a). The three vibrational states $\nu = 1$, 2, and 3 amount to around 50% of the total population. Figure 2(b) shows the wave function for all these 19 vibrational states, and Figure 2(c) plots $|\psi_g(R,t)|^2$ obtained under $E(t) = 0$. The black curve in Figure 2(c) is the expected time-dependent internuclear distance $\langle R(t)\rangle$. Clearly, the NWP goes through a collapse and revival procedure, and the revival time is about 300 fs [15,17].

2.2. Numerical optimisation algorithm

We formulate the design of a laser field E to realise the NWP transfer of ψ_g as a minimax problem, and then apply a sequential linear programming algorithm to solve it. To avoid ionisation of H_2^+, we restrict the amplitude of E within 0.1, and the pulse duration less than 32 fs. Note that the pulse designed before was usually several hundred femtoseconds [47–50].

In the case when there are no constraints on the laser pulses, one can apply optimal control algorithms with Lagrange multiplier [53,54], or the monotonically convergent algorithm [55], or the Krotov-type algorithm [56,57]. These algorithms are developed in the theoretical chemistry and molecular physics communities in the past 25 years and are highly efficient in finding control pulses. However, when the control pulses are constrained, these algorithms may not be applied directly. One can add an *ad hoc* saturation step; however, this may significantly slow down the optimisation convergence. Another method is to supplement a penalty term to the cost function to prevent the constraints from being violated, but there is no guarantee that the algorithms will yield a feasible solution. In this paper, we will formulate the control pulse design as a constrained minimax problem and then apply sequential linear programming to solve it [51]. The major advantage of this algorithm is that

it can explicitly deal with the case when the control pulses are constrained.

The wave function transfer is formulated as a constrained minimax problem on the laser electric field E:

$$\min_{E} \max_{n\in\{0,1,\ldots,N-1\}} J_n, \tag{4}$$

subject to

$$|E(t_k)| \le 0.1,\ k = 0, \ldots, K-1, \tag{5}$$

where

$$J_n = \frac{1}{2}\left\|\psi_g^0(R_n) - e^{-i\alpha}\psi_g(R_n, T_f)\right\|^2. \tag{6}$$

Here n (or k) is the index for the spatial (or temporal) step, N (or K) is the total points in the spatial (or temporal) axis, and α is a global phase to be determined soon. The function J_n quantifies the difference between the desired and actually achieved wave functions at the spatial grid R_n. If the maximum error of J_n is minimised over the whole spatial range, one can expect that the desired wave function is achieved.

The NWP transfer fidelity $|F|^2$ can be measured by defining

$$F = \mathrm{Re}\left\{e^{i\alpha}\left\langle\psi_g(R, T_f)|\psi_g^{v=0}(R)\right\rangle\right\}. \tag{7}$$

The global phase α in Equations (6) and (7) can be obtained by maximising the fidelity:

$$\alpha = -\arg\left\{\left\langle\psi_g(R, T_f)|\psi_g^{v=0}(R)\right\rangle\right\}, \tag{8}$$

where arg denotes the argument of a complex number.

The minimax problem has been extensively studied in the optimisation and control community [58–60]. To find the optimal laser field, we start from an initial guess and then gradually approach the optimal solution by iteration. Suppose that at the jth iteration, the current laser pulse is E^j. We need to determine a small increment ΔE^j such that at the $(j+1)$th step, the new laser pulse $E^{j+1} = E^j + \Delta E^j$ is a better solution to minimise the transfer error J_n. In the first-order approximation, we have

$$J_n(E^{j+1}) \approx J_n(E^j) + \nabla_{E^j}^T J_n(E^j)\Delta E^j. \tag{9}$$

The analytic derivation of the gradient $\nabla_{E^j}^T J_n(E^j)$ is given in the appendix.

We then apply a sequential linear programming algorithm as follows:

(1) *Choose a small constant as the initial guess of the electric field;*
(2) *At the* j*th step, compute* $\mathrm{J_n}(E^j)$ *and* $\nabla_{E^j} J_n(E^j)$*;*
(3) *Determine the increment* ΔE^j *from the following linear programming problem:*

$$\min_{\Delta E^j} \gamma,$$

subject to

$$\begin{aligned}
&\nabla_{E^j}^T J_0(E^j)\Delta E^j + J_0(E^j) \le \gamma,\\
&\qquad\vdots\\
&\nabla_{E^j}^T J_{N-1}(E^j)\Delta E^j + J_{N-1}(E^j) \le \gamma,\\
&-0.1 - E^j \le \Delta E^j \le 0.1 - E^j.
\end{aligned} \tag{10}$$

(4) *Let* $E^{j+1} = E^j + \epsilon\Delta E^j$*, where* ϵ *is a small positive number controlling the step size;*
(5) *Repeat Steps* (2)–(4) *until a desired convergence is reached.*

Note that in each iteration, we only need to solve a linear programming problem, which can be readily calculated by numerical packages. This algorithm can also be extended to deal with other types of restrictions. For instance, we can convert a linear matrix inequality constraint $AE \le b$ into $A\Delta E^j \le b - AE^j$ and then add it directly into the constraints (10) of the sequential linear programming. For a nonlinear constraint $g(E) \le d$, we can expand it at the current E^j and obtain the approximative constraint $\nabla_{E^j}^T g(E^j)\Delta E^j \le d - g(E^j)$. This is again a linear constraint and can be added into Equation (10).

3. Optimal design results

Starting from $E(t) = 0.01$, after around 12,000 iterations and 350+ hours computation on a desktop computer with Intel i5 CPU, we have obtained a satisfactory optimal laser pulse as shown in Figure 3(a). The initial guess of the electric field can be other forms, such as the Gaussian or $\sin^2$ profile. However, we use a small constant as the initial guess because we chose to not assume any prior knowledge about the transition between the two electronic states before the optimisation. One may expect that a proper initial guess of the laser pulse may expedite the convergence of the optimisation. Figure 3(b)–(d) show the optimal laser pulse induced NWP evolution for $|\psi_g(R, t)|^2$, $|\psi_u(R, t)|^2$, and $|\psi_g(R, t)|^2 + |\psi_u(R, t)|^2$, respectively.

Figure 3(a) reveals an interesting physical story. First of all, the optimal laser field is a pulse train. After the inception of H_2^+, nearly no electric field is introduced until $t = 11$ fs. In this period, the NWP propagates freely to the outer turning point and then turns back, as shown in Figure 3(b). The main pulse appears at around $t = 11$ fs, at which time the NWP is moving inward instead of outward. This is important because if the laser field starts interacting with the NWP when it is moving outward, the part of the wave packets

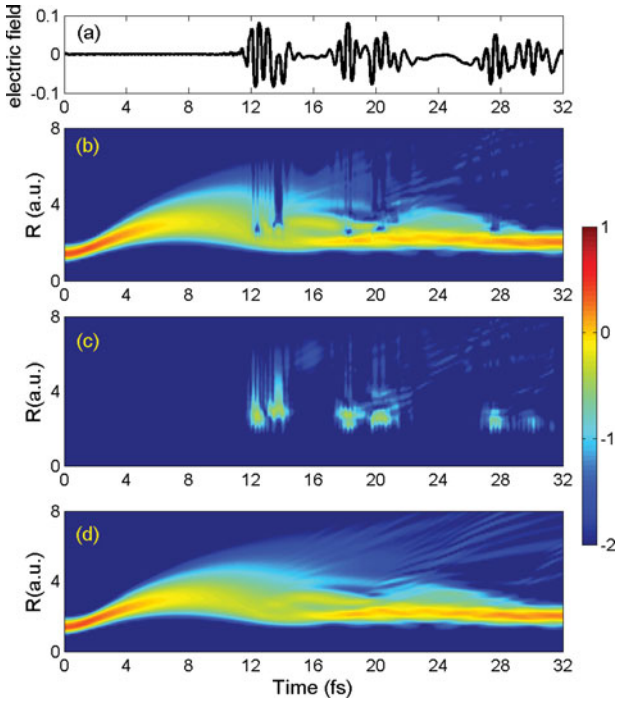

Figure 3. (Colour online) (a) The designed optimal laser pulse train. The evolution of $|\psi_g(R, t)|^2$ (b), $|\psi_u(R, t)|^2$(c), and $|\psi_g(R, t)|^2 + |\psi_u(R, t)|^2$ (d) (all in logarithmic scale).

promoted to $2p\sigma_u$ surface will directly dissociate and the subsequent laser pulse has little chance to pull them back to the bound states [48].

To transfer $\psi_g(R, t)$ to $\psi_g^{v=0}(R)$, $\psi_u(R, t)$ must be an intermediate state. From a closer look at Figure 3(b) and (c), one may find that within each oscillation of the electric field, part of ψ_g and ψ_u are exchanged. The wave function $\psi_u(R, t)$ mainly distributes close to the range $R = 3$. The quantity $|\psi_g(R, t)|^2 + |\psi_u(R, t)|^2$ gives a smooth evolution of the NWP, as depicted in Figure 3(d). At the terminal time, the NWP has been transferred to the ground vibrational state.

To gain a deeper understanding of the transfer principle, we trace the time-dependent probability evolution of each individual vibrational state, which can be written as

$$P_v(t) = \left|\langle\psi_g^v(R)|\psi_g(R, t)\rangle\right|^2, \quad \text{for } v = 0, \ldots, 18. \quad (11)$$

Figure 4 shows $P_v(t)$ for the first seven vibrational states. It is clear that the population of $v = 0$ increases to 91% at the end of the evolution, and the staircase jumps take place at the times when the laser pulse is introduced. The quick increasing of the ground-state population and the precipitous dropping of the excited vibrational states indicate that the laser-induced coupling is roughly an anti-Stokes transition: H_2^+ with higher nuclear vibrational states is excited from $1s\sigma_g$ to $2p\sigma_u$, and then de-excited to $1s\sigma_g$ with lower nuclear vibrational states. The probability evolution details show more physical scenarios. At the beginning $v = 1$ and

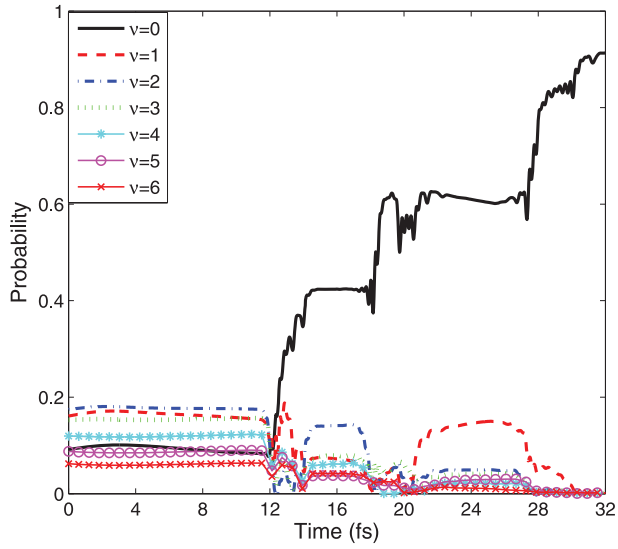

Figure 4. (Colour online) The time-dependent probabilities for the lowest 7 vibrational states.

$v = 2$ states have similar probabilities. After the first laser pulse, the probability of $v = 1$ is halved, whereas the probability of $v = 2$ does not change much. Surprisingly, after the second pulse, the probability of $v = 1$ is doubled and is much larger than that of $v = 2$. After these two pulses, the vibrational states with $v \geq 2$ are already very small, and the upcoming third pulse mainly transfers $v = 1$ to $v = 0$. During the whole process, $v = 1$ state works as a temporary reservoir for storing some populations, for ultimately maximising the population of $v = 0$.

The frequency spectrum of the obtained laser pulse train is shown in Figure 5 after performing the Fourier transform. The main frequency component is around 0.25 (corresponding to the wavelength 182 nm). This is consistent with the

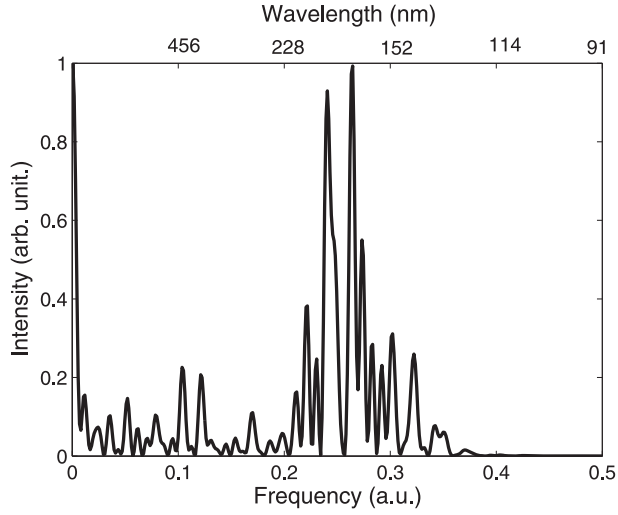

Figure 5. The frequency spectrum for the designed optimal laser pulse train.

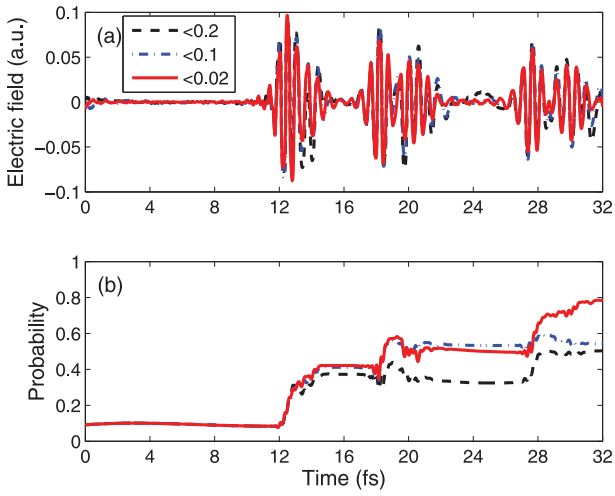

Figure 6. (a) The laser field after filtering out the low frequency components. (b) The time-dependent probabilities induced by the laser fields in (a).

optimisation result in Figure 3(c), where $\psi_u(R)$ is mainly excited at the internuclear distance between 2.5 to 3, for the energy gap between $1s\sigma_g$ and $2p\sigma_u$ at the corresponding internuclear distance is around 0.25. The frequency analysis demonstrates that the multi-frequency laser pulse train pumps and dumps H_2^+ with different frequency components.

The optimised laser field has a very wide frequency spectrum, which is difficult to be realised in the experiment. To obtain a more realistic laser field, we filter out the very low frequency components from the optimised laser field. Figure 6 shows (a) the laser field after filtering the frequency components that is <0.2 (black dashed line), <0.1 (blue dash-dotted line), and <0.02 (red solid line), and (b) the corresponding probability evolutions of the ground vibrational state. The final probability of the ground vibrational state is 0.5, 0.54, 0.79. Such optimisation results are already good enough for many physical studies. We expect the incremental improvements of the pulse shaping technology[61–63] may experimentally generate such an optimised laser pulse in the near future.

4. Discussions and conclusions

In the experiment, the H_2^+ molecular beam may be generated through the field- or impact-ionisation of H_2. In the impact-ionisation of H_2, the nuclear vibrational wave packets of the generated molecular beam H_2^+ may be incoherent[64] when the laser field is acted on. In this paper, we only consider the H_2^+ generated from the field-ionisation, in which case the nuclear wave packets of H_2^+ are fully coherent. Experimentally, the focused laser pulse has the intensity distribution in space, and the different intensities affect the tunnelling ionisation seriously. Further, the field-ionisation tends to generate the H_2^+ with cooler vibration states than those described by the Franck–Condon approximation. Therefore, to describe the nuclear wave packet more precisely, it is better to count on the focal volume averaging [65] and use the MO-ADK [66] approximation. However, this tedious calculation may be evaded in the attosecond-pump and femtosecond-probe experiment[67], and the control strategy does not care much about the initial wave function. The wide frequency spectra of the attosecond pulse may kick off one of the electrons in H_2 quickly enough, and generate the H_2^+ with the NWP distribution well described by the Franck–Condon approximation.

To get a more realistic laser pulse, one may set more restrictions in the optimisation algorithm, for example, confining the frequencies within a certain range. However, more restrictions will make the computation time longer. One way to possibly reduce the calculation time is to give a better initial guess for the laser pulse to be optimised, though which assumes some transferring mechanisms are known. In this paper, we set the initial field as a constant by assuming that nothing about the molecular ion has already been known, and we demonstrate it is possible to optimise a laser pulse train to transfer the coherent nuclear vibrational states to the ground vibrational eigenstate.

In conclusion, by restricting the laser pulse duration to less than 32 fs and confining the electric amplitude within 0.1, we numerically design an optimal laser pulse train to successfully transfer the initial Franck–Condon NWP to the ground vibrational state of H_2^+ with a population 91%, and the dissociation probability is only 9%. As far as we know, we obtain the highest transition rate when the driving laser field is limited to dozens of femtoseconds. The optimal laser pulse train does not act on the NWP until the NWP is moving inward. The field-induced Raman transition between $1s\sigma_g$ and $2p\sigma_u$ transfers the highly excited vibrational states to $\nu = 0$ directly, or indirectly first to $\nu = 1$ but finally to $\nu = 0$ state. This control algorithm can be extended to other molecules.

Acknowledgements

JZ, GQH, and FH thank the financial support from NSFC (No. 61174086, 61102053, 11104180, 11175120, 11121504, 11322438), and Project-sponsored by SRF for ROCS SEM. JZ and FH thank the Shanghai Pujiang scholar funding (No. 11PJ1405800, 11PJ1404800), and State Key Laboratory of Precision Spectroscopy, ECNU, China. JZ thanks the Innovation Program of Shanghai Municipal Education Commission (No. 11ZZ20). GQH thanks the SMC Excellent Young Faculty Award. FH thanks the NSF of Shanghai (No. 11ZR1417100) and the Fok Ying-Tong Education Foundation for Young Teachers in the Higher Education Institutions of China (No. 131010).

References

[1] F. Krausz and M. Ivanov, Rev. Mod. Phys. **81**, 163 (2009).
[2] M. Lein, J. Phys. B **40**, R135 (2007).

[3] W. Becker, X. Liu, P. Ho, and J.H. Eberly, Rev. Mod. Phys. **84**, 1011 (2012).

[4] A. Becker, F. He, A. Picon, C. Ruiz, N. Takemoto, and A. Jaron-Becker, in *Springer Series in Optical Sciences*, edited by L. Plaja, R. Torres, and A. Zair (Springer, Berlin - Heidelberg, 2013), Vol. 177, pp. 207–229.

[5] M. Shapiro and P. Brumer, *Quantum Control of Molecular Processes* (Wiley-VCH, New York, 2011).

[6] D.J. Tannor and S.A. Rice, J. Chem. Phys. **83**, 5013 (1985).

[7] S. Shi, A. Woody, and H. Rabitz, J. Chem. Phys. **88**, 6870 (1988).

[8] A. Baltuska, T. Udem, M. Uiberacker, M. Hentschel, E. Goulielmakis, C. Gohle, R. Holzwarth, V.S. Yakovlev, A. Scrinzi, T.W. Hänsch, and F. Krausz, Nature (London) **421**, 611 (2003).

[9] G.G. Paulus, F. Grasbon, H. Walther, P. Villoresi, M. Nisoli, S. Stagira, E. Priori, and S. De Silvestri, Nature (London) **414**, 182 (2001).

[10] V. Roudnev, B.D. Esry, and I. Ben-Itzhak, Phys. Rev. Lett. **93**, 163601 (2004).

[11] M.F. Kling, Ch. Siedschlag, A.J. Verhoef, J.I. Khan, M. Schultze, Th. Uphues, Y. Ni, M. Uiberacker, M. Drescher, F. Krausz, and M.J.J. Vrakking, Science **312**, 246 (2006).

[12] F. He, C. Ruiz, and A. Becker, Phys. Rev. Lett. **99**, 083002 (2007).

[13] M. Uiberacker, Th. Uphues, M. Schultzelink, A.J. Verhoef, V. Yakovlevlink, M.F. Klinglink, J. Rauschenberger, N.M. Kabachnik, H. Schröder, M. Lezius, K.L. Kompa, H.G. Mller, M.J.J. Vrakking, S. Hendel, U. Kleineberglink, U. Heinzmann, M. Drescher, and F. Krausz, Nature **446**, 627 (2007).

[14] G. Sansone, F. Kelkensberg, J.F. Perez-Torres, F. Morales, M.F. Kling, W. Siu, O. Ghafur, P. Johnsson, M. Swoboda, E. Benedetti, F. Ferrari, F. Lepine, J.L. Sanz-Vicario, S. Zherebtsov, I. Znakovskaya, A. LHuillier, M. Yu. Ivanov, M. Nisoli, F. Martin, and M.J.J. Vrakking, Nature (London) **465**, 763 (2010).

[15] Th. Ergler, B. Feuerstein, A. Rudenko, K. Zrost, C.D. Schröter, R. Moshammer, and J. Ullrich, Phys.Rev. Lett. **97**, 103004 (2006).

[16] G.H. Dunn, Phys. Rev. **172**, 1 (1968).

[17] B. Feuerstein and U. Thumm, Phys. Rev. A **67**, 063408 (2003).

[18] A. Requate, A. Becker, and F.H.M. Faisal, Phys. Rev. A **73**, 033406 (2006).

[19] U. Thumm, T. Niederhausen, and B. Feuerstein, Phys. Rev. A **77**, 063401 (2008).

[20] A.D. Bandrauk and M.L. Sink, J. Chem. Phys. **74**, 1110 (1981).

[21] P.H. Bucksbaum, A. Zavriyev, H.G. Muller, and D.W. Schumacher, Phys. Rev. Lett. **64**, 1883 (1990).

[22] A. Giusti-Suzor, X. He, O. Atabek, and F.H. Mies, Phys. Rev. Lett. **64**, 515 (1990).

[23] L.J. Frasinski, J.H. Posthumus, J. Plumridge, K. Codling, P.F. Taday, and A.J. Langley, Phys. Rev. Lett. **83**, 3625 (1999).

[24] M. Kremer, B. Fischer, B. Feuerstein, V.L.B. de Jesus, V. Sharma, C. Hofrichter, A. Rudenko, U. Thumm, C.D. Schröter, R. Moshammer, and J. Ullrich, Phys. Rev. Lett. **103**, 213003 (2009).

[25] B. Fischer, M. Kremer, T. Pfeifer, B. Feuerstein, V. Sharma, U. Thumm, C.D. Schröter, R. Moshammer, and J. Ullrich, Phys. Rev. Lett. **105**, 223001 (2010).

[26] K.P. Singh, F. He, P. Ranitovic, W. Cao, S. De, D. Ray, S. Chen, U. Thumm, A. Becker, M.M. Murnane, H.C. Kapteyn, I.V. Litvinyuk and C.L. Cocke, Phys. Rev. Lett. **104**, 023001 (2010).

[27] F. He, A. Becker, and U. Thumm, Phys. Rev. Lett. **101**, 213002 (2008).

[28] F. He, Phys. Rev. A **86**, 063415 (2012).

[29] F. He, C. Ruiz, and A. Becker, J. Phys. B **41**, 081003 (2008).

[30] F. He and A. Becker, J. Phys. B **41**, 074017 (2008).

[31] K. Liu, Q. Zhang, and P. Lu, Phys. Rev. A **86**, 033410 (2012).

[32] P. Lan, E.J. Takahashi, and K. Midorikawa, Phys. Rev. A **86**, 013418 (2012).

[33] F. Anis and B.D. Esry, Phys. Rev. Lett. **109**, 133001 (2012).

[34] T. Zuo and A.D. Bandrauk, Phys.Rev. A **52**, R2511 (1995).

[35] D. Pavicic, A. Kiess, T.W. Hansch, and H. Figger, Phys. Rev. Lett. **94**, 163002 (2005).

[36] I.A. Bocharova, H. Mashiko, M. Magrakvelidze, D. Ray, P. Ranitovic, C.L. Cocke, and I.V. Litvinyuk, Phys. Rev. A **77**, 053407 (2008).

[37] B. Manschwetus, T. Nubbemeyer, K. Gorling, G. Steinmeyer, U. Eichmann, H. Rottke, and W. Sandner, Phys. Rev. Lett. **102**, 113002 (2009).

[38] A. Staudte, D. Pavicic, S. Chelkowski, D. Zeidler, M. Meckel, H. Niikura, M. Schöffler, S. Schössler, B. Ulrich, P.P. Rajeev, Th. Weber, T. Jahnke, D.M. Villeneuve, A.D. Bandrauk, C.L. Cocke, P.B. Corkum, and R. Dörner, Phys. Rev. Lett. **98**, 073003 (2007).

[39] H. Niikura, F. Legare, R. Hasbani, M.Y. Ivanov, D.M. Villeneuve, and P.B. Corkum, Nature (London) **421**, 826 (2003).

[40] X.M. Tong, Z.X. Zhao, and C.D. Lin, Phys. Rev. Lett. **91**, 233203 (2003).

[41] C.C. Chirila and M. Lein, Phys. Rev. A **77**, 043403 (2008).

[42] S. Saugout, C. Cornaggia, A. Suzor-Weiner, and E. Charron, Phys. Rev. Lett. **98**, 253003 (2007).

[43] F. Kelkensberg, W. Siu, J.F. Perez-Torres, F. Morales, G. Gademann, A. Rouzee, P. Johnsson, M. Lucchini, F. Calegari, J.L. Sanz-Vicario, F. Martin, and M.J.J. Vrakking, Phys. Rev. Lett. **107**, 043002 (2011).

[44] J. McKenna, F. Anis, B. Gaire, N.G. Johnson, M. Zohrabi, K.D. Carnes, B.D. Esry, and I. Ben-Itzhak, Phys. Rev. Lett. **103**, 103006 (2009).

[45] H. Niikura, D.M. Villeneuve, and P.B. Corkum, Phys. Rev. A **73**, 021402(R) (2006).

[46] P.A. Orr, I.D. Williams, J.B. Greenwood, I.C.E. Turcu, W.A. Bryan, J. Pedregosa-Gutierrez, and C.W. Walter, Phys. Rev. Lett. **98**, 163001 (2007).

[47] T. Niederhausen and U. Thumm, Phys. Rev. A **77**, 013407 (2008).

[48] H. Niikura, D.M. Villeneuve, and P.B. Corkum, Phys. Rev. Lett. **92**, 133002 (2004).

[49] A. Picon, J. Biegert, A. Jaron-Becker, and A. Becker, Phys. Rev. A **83**, 023412 (2011).

[50] W.A. Bryan, C.R. Calvert, R.B. King, G.R.A.J. Nemeth, J.D. Alexander, J.B. Greenwood, C.A. Froud, I.C.E. Turcu, E. Springate, W.R. Newell, and I.D. Williams, Phys. Rev. A **83**, 021406 (R) (2011).

[51] J. Zhang and R. Kosut, IEEE Trans. Contr. Syst. Technol. **21**, 869 (2013).

[52] M.D Feit, J.A Fleck, Jr., and A Steiger, J. Comp. Phys. **47**, 412 (1982).

[53] A.P. Peirce, M.A. Dahleh, and H. Rabitz, Phys. Rev. A **37**, 4950 (1988).

[54] R. Kosloff, S.A. Rice, P. Gaspard, S. Tersigni, and D.J. Tannor, Chem. Phys. **139**, 201 (1985).

[55] W. Zhu, J. Botina, and H. Rabitz, J. Chem. Phys. **108**, 1953 (1998).
[56] D.J. Tannor, V.A. Kazakov, and V. Orlov, in *Time-dependent Quantum Molecular Dynamics*, edited by J. Broeckhove and L. Lathouwers, NATO ASI Series B: Physics, **299**, 347 (1992).
[57] J. Somloi, V.A. Kazakov, and D.J. Tannor, Chem. Phys. **172**, 85 (1993).
[58] J.W. Bandler, T.V. Srinivasan, and C. Charalambous, IEEE Trans. Microwave Theory Tech. **20**, 596 (1972).
[59] J. Hald and K. Madsen, Math. Program. **20**, 49 (1981).
[60] A.R. Conn and Y. Li, SIAM J. Optim. **2**, 242 (1992).
[61] S. Zhdanovich, E.A. Shapiro, M. Shapiro, J.W. Hepburn, and V. Milner, Phys. Rev. Lett. **100**, 103004 (2008).
[62] B.C. Chen and S.H. Lim, J. Phys. Chem. B **112**, 3653 (2008).
[63] A. Monmayrant, S. Weber, and B. Chatel, J. Phys. B **43**, 103001 (2010).
[64] I. Ben-Itzhak, P.Q. Wang, J.F. Xia, A.M. Sayler, M.A. Smith, K.D. Carnes, and B.D. Esry, Phys. Rev. Lett. **95**, 073002 (2005).
[65] R. Kopold, W. Becker, M. Kleber, and G.G. Paulus, J. Phys. B **35**, 217 (2002).
[66] X.M. Tong, Z.X. Zhao, and C.D. Lin, Phys. Rev. A **66**, 033402 (2002).
[67] K.P. Singh, F. He, P. Ranitovic, W. Cao, S. De, D. Ray, S. Chen, U. Thumm, A. Becker, M.M. Murnane, H.C. Kapteyn, I.V. Litvinyuk, and C.L. Cocke, Phys. Rev. Lett. **104**, 023001 (2010).
[68] D.J. Tannor, *Introduction to Quantum Mechanics* (University Science Books, Sausalito, CA, 2007).
[69] P. Schwendner, F. Seyl, and R. Schinke, Chem. Phys. **217**, 233 (1997).

Appendix. Derivation of $\nabla_{E^j} J_n$

For completeness, we first briefly describe the numerical procedure to solve the Schrödinger equation Equation (1). We follow the journal split-operator techniques in Refs. [52,68,69]. Let

$$E = [E_0, E_1, \ldots, E_{K-1}], \quad R = [R_0, R_1, \ldots, R_{N-1}].$$

The solution of Equation (1) can be written as

$$\psi(R, T_f) = \prod_{k=0}^{K-1} e^{-iH_k \Delta t} \psi(R, 0), \tag{A1}$$

where

$$H_k = \begin{pmatrix} T_R + V_g & d_{gu}(R)E_k \\ d_{gu}(R)E_k & T_R + V_u(R) \end{pmatrix} \tag{A2}$$

which is decomposed as

$$H_k = T + G_k,$$

where

$$T = \begin{pmatrix} T_R & 0 \\ 0 & T_R \end{pmatrix}, \quad G_k = \begin{pmatrix} V_g(R) & d_{gu}(R)E_k \\ d_{gu}(R)E_k & V_u(R) \end{pmatrix}. \tag{A3}$$

The propagation operator $e^{-iH_k \Delta t}$ in Equation (A1) can be calculated by the split-operator method:

$$e^{-iH_k \Delta t} = e^{-iT\frac{\Delta t}{2}} e^{-iG_k \Delta t} e^{-iT\frac{\Delta t}{2}} + O(\Delta t^3). \tag{A4}$$

Substitution of Equation (A4) into Equation (A1) yields

$$\psi(R, T_f) = e^{-iT\frac{\Delta t}{2}} \left(\prod_{k=0}^{K-1} e^{-iG_k \Delta t} e^{-iT\Delta t} \right) e^{iT\frac{\Delta t}{2}} \psi(R, 0). \tag{A5}$$

Here the terms $e^{-iT\frac{\Delta t}{2}}$ and $e^{-iT\Delta t}$ can be calculated by Fast Fourier Transform (FFT) [68]. Since all the four blocks in G_k are diagonal matrices, we can transform G_k into a block diagonal matrix $\tilde{G}_k = \mathrm{diag} G_k^0, G_k^1, \ldots, G_k^{N-1}$, where

$$G_k^n = \begin{pmatrix} V_g(R_n) & d_{gu}(R_n)E_k \\ d_{gu}(R_n)E_k & V_u(R_n). \end{pmatrix} \tag{A6}$$

Because G_k^n is symmetric, it can be derived that

$$e^{-iG_k^n \Delta t} = \exp\left\{ -i \frac{V_g(R_n) + V_u(R_n)}{2} \Delta t \right\} \left\{ \cos\frac{\theta_k \Delta t}{2} I - i \sin\frac{\theta_k \Delta t}{2} \left(\frac{V_g(R_n) - V_u(R_n)}{\theta_k} \sigma_z + \frac{2 d_{gu}(R_n) E_k}{\theta_k} \sigma_x \right) \right\}, \tag{A7}$$

where σ_x, σ_z are Pauli matrices, and

$$\theta_k = \sqrt{(V_g(R_n) - V_u(R_n))^2 + (2 d_{gu}(R_n) E_k)^2}. \tag{A8}$$

This completes the numerical solution of Equation (1).

Now from Equation (6), we have

$$\nabla_E J_n = -\mathrm{Re}\left\{ \left(\overline{\psi_g^0}(R_n) - e^{i\alpha} \overline{\psi_g}(R_n, T_f) \right) \times \nabla_E (e^{-i\alpha} \psi_g(R_n, T_f)) \right\}. \tag{A9}$$

For an element E_k in the vector E, it is easy to get

$$\frac{\partial}{\partial E_k} e^{-i\alpha} \psi_g(R_n, T_f) = e^{-i\alpha} \frac{\partial}{\partial E_k} \psi_g(R_n, T_f) - e^{-i\alpha} \psi_g(R_n, T_f) \frac{\partial \alpha}{\partial E_k}. \tag{A10}$$

From Equation (A5), we obtain that

$$\frac{\partial}{\partial E_k} \psi(R, T_f) = e^{-iT\frac{\Delta t}{2}} \left(\prod_{l=k+1}^{K-1} e^{-iG_l \Delta t} e^{-iT\Delta t} \right) \times \frac{\partial}{\partial E_k} e^{-iG_k \Delta t} e^{-iT\Delta t} \left(\prod_{l=0}^{k-1} e^{-iG_l \Delta t} e^{-iT\Delta t} \right) \times e^{iT\frac{\Delta t}{2}} \psi(R, 0).$$

From Equations (A7) and (A8), it follows that

$$\frac{\partial}{\partial E_k} e^{-iG_k^n \Delta t} = \frac{\partial}{\partial \theta_k} e^{-iG_k^n \Delta t} \frac{\partial \theta_k}{\partial E_k} + \frac{\partial}{\partial E_k} e^{-iG_k^n \Delta t}.$$

Proceeding further, we obtain

$$\begin{aligned}\frac{\partial}{\partial \theta_k} e^{-iG_k^n \Delta t} = e^{-i\frac{V_g+V_u}{2}\Delta t} \Bigg\{ & -\frac{\Delta t}{2} \sin\frac{\theta_k \Delta t}{2} I \\ & -\frac{i\Delta t}{2} \cos\frac{\theta_k \Delta t}{2} \left(\frac{V_g - V_u}{\theta_k} \sigma_z + \frac{2d_{gu}E_k}{\theta_k} \sigma_x \right) \\ & + i \sin\frac{\theta_k \Delta t}{2} \left(\frac{V_g - V_u}{\theta_k^2} \sigma_z + \frac{2d_{gu}E_k}{\theta_k^2} \sigma_x \right) \Bigg\},\end{aligned}$$

and

$$\begin{aligned}\frac{\partial \theta_k}{\partial E_k} &= \frac{4d_{gu}^2 E_k}{\theta_k}, \\ \frac{\partial}{\partial E_k} e^{-iG_k^n \Delta t} &= -ie^{-i\frac{V_g+V_u}{2}\Delta t} \sin\frac{\theta_k \Delta t}{2} \frac{2d_{gu}}{\theta_k} \sigma_x.\end{aligned}$$

Lastly, we need to calculate $\frac{\partial \alpha}{\partial E_k}$ in Equation (A10). Rereading Equation (8) and defining

$$\begin{aligned}p &= \mathrm{Re}\left\{ \sum_{n=0}^{N-1} \psi_g^0(R_n) \overline{\psi_g(R_n, T_f)} \right\}, \\ q &= \mathrm{Im}\left\{ \sum_{n=0}^{N-1} \psi_g^0(R_n) \overline{\psi_g(R_n, T_f)} \right\},\end{aligned}$$

we obtain

$$\frac{\partial \alpha}{\partial E_k} = \frac{1}{p^2 + q^2} \left(p \frac{dq}{dE_k} - q \frac{dp}{dE_k} \right),$$

where $\frac{dp}{dE_k}$ and $\frac{dq}{dE_k}$ are none other than the real and imaginary parts of the quantity

$$\sum_{n=0}^{N-1} \psi_g^0(R_n) \frac{\partial}{\partial E_k} \overline{\psi_g(R_n, T_f)}.$$

Combining all these equations, we can calculate $\nabla_{E^j} J_n$ in an explicit manner.